

# Effects of Reactive Oxygen Species on Single Polycation Layers

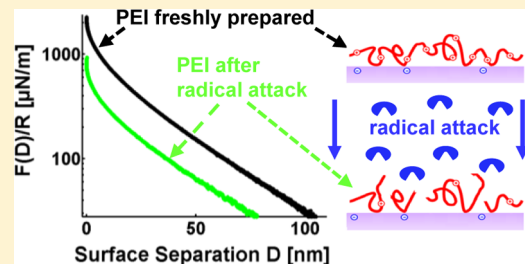
Florian Berg,<sup>†</sup> Stephan Block,<sup>‡</sup> Steffen Drache,<sup>†</sup> Rainer Hippler,<sup>†</sup> and Christiane A. Helm\*,<sup>†</sup>

<sup>†</sup>Institut für Physik, Ernst-Moritz-Arndt Universität, Felix-Hausdorff-Str. 6, 17489 Greifswald, Germany

<sup>‡</sup>ZIK HIKE—Zentrum für Innovationskompetenz Humorale Immunreaktionen bei kardiovaskulären Erkrankungen, Fleischmannstr. 42 – 44, 17475 Greifswald, Germany

## Supporting Information

**ABSTRACT:** Positively charged, branched polyethylenimine (PEI) adsorbed onto silicon wafers and silica surfaces are attacked by free hydroxyl radicals. With AFM colloid probe technique, the surface forces between PEI layers are measured. Force profiles show that an electrostatic repulsion dominates the surface forces between freshly deposited PEI layers. After radical attack, both surface potential and surface charge density are reduced by a factor of about 0.5, while the Debye length remains unchanged. Adsorbed gold nanoparticles and force volume measurements show a homogeneous distribution of the surface charge on length scales between 40 nm and 30  $\mu\text{m}$ . For radical attacked PEI layers, we find a 10% decrease of saturation coverage of gold nanoparticles. This is consistent with the decreased surface charge density, if the electrostatic three-body interaction is taken into account. Nevertheless, the NP adsorption kinetics are slowed down suggesting that the PEI layer is inhomogeneous on the nm-scale after radical attack.



## INTRODUCTION

Biological systems are constantly exposed to reactive oxygen species (ROS) because ROS are byproducts of the normal metabolism. Other sources of ROS are irradiation (esp. UV light) and also chemical reactions involving transition metal ions.<sup>1–3</sup> ROS are known to play an important role in many pathological pathways, in cancer development, aging, etc.<sup>1,3</sup> While ROS in biochemical pathways have attracted much attention, their effects are examined by techniques solely sensitive on the molecular level, such as electrochemistry or spectroscopy.<sup>4</sup> However, the ROS treatment also affects the self-organization of molecules and the inter- and intramolecular interactions. Here, we explore the stability of a polymer layer after ROS attack. We want to elucidate if the molecular changes induced by ROS are homogeneous on the nm- and  $\mu\text{m}$ -scale.

A reactive oxygen radical induces a chemical reaction. Many different reactions have been reported. For instance, a functional group is cleaved from an organic surface or a OH group is added.<sup>1,5</sup> These reactions occur on a molecular length scale, on a nm-sized spot. Recently, we investigated the reaction of zwitterionic lipid monolayers with ROS.<sup>5</sup> In contrast to the adsorbed polymer layer investigated in this paper, the lipid monolayer is expected to be homogeneous on the  $\mu\text{m}$ -length scale after the reactions with ROS, since the lipids diffuse laterally and mix.

Our approach is to adsorb polyelectrolytes onto an oppositely charged solid substrate and to expose this surface to ROS. In water, most substrates are negatively charged (silica, glass, mica, etc.), which suggests using polycations. Often, the adsorption of a polycation onto a substrate is an irreversible nonequilibrium process, leading to charge reversal.<sup>6–8</sup> Those monomers, which form an electrostatic bond with the substrate,

remain flatly adsorbed and immobilized independent of the composition of the aqueous solution. Only the fraction of chains, which protrude into the solution, swell and shrink in dependence of the salt concentration.<sup>9</sup> Therefore, if reactions with ROS destroy the electrostatic bonds that attach the polymer to the substrate, chains which protrude into the solution can be detected by changes in the surface forces.

We measure the surface charge with AFM, using the colloid probe (CP) technique. With this approach, the surface charge is averaged over the length scale of the CP, which is usually the  $\mu\text{m}$ -scale. To ensure that the surface forces are due to electrostatic forces only and to avoid steric forces, flatly adsorbed polycations are used. This conformation is obtained by adsorption from salt-free solution and usage of the branched polycation poly(ethylene imine) (PEI).<sup>6–8,10</sup> We hope that even after the cleavage of positively charged side groups the PEI remains flatly bound to the surface enabling reliable quantification of changes in surface charge and surface potential.

The lateral homogeneity of the surface charge is probed with spatially resolved force measurements on the length scale of up to 30  $\mu\text{m}$  (force volume mode). To probe the lateral homogeneity on the nm-scale, gold nanoparticles (AuNPs, diameter 16 nm) are adsorbed. Both the adsorption kinetics and the surface coverage of the AuNP are analyzed. To understand the relation between surface charge and the maximum coverage of the AuNPs, an extended three-body RSA (random sequential adsorption) model is applied.<sup>11,12</sup>

Received: December 24, 2012

Revised: May 17, 2013

Published: June 20, 2013

## MATERIALS AND METHODS

**Materials.** Branched polycation poly(ethylene imine) (PEI;  $M_w = 75$  kDa) was purchased from Sigma Aldrich (München, Germany). Fenton's reagent is made from 5 mM EDTA (ethylenediaminetetraacetic acid; Sigma Aldrich), 4 mM Mohr's salt (ammonium iron(II) sulfate, Merck, Darmstadt, Germany), and 0.1 M  $H_2O_2$  (hydrogen peroxide, Roth, Karlsruhe, Germany). The molar ratio between EDTA and  $Fe^{2+}$  is set to 5:4 and the molar ratio between  $Fe^{2+}$  and  $H_2O_2$  to 1:3. Negatively charged colloidal gold nanoparticles (AuNPs) synthesized according to Turkevich et al.<sup>13</sup> (diameter  $\sim 16$  nm, AuNP concentration 2.4 nM, Debye length 3.89 nm) are used as marker particles.<sup>14</sup> All chemicals are of analytical grade and are used without further purification.

All solutions are prepared with deionized, ultrapure water using a Milli-Q water purification device (Millipore, Billerica, MA). Microscope slides (Roth, Karlsruhe, Germany; made of soda-lime glass containing >75% silica) or polished surfaces of Si (100) wafers (Matthias Schmehl, Rostock, Germany) served as negatively charged substrates.

All AFM images and force measurements are obtained with a DI Multimode equipped with a Nanoscope IIIa controller (Digital Instruments, Santa Barbara, CA). For AFM imaging OMCL-AC160TS cantilevers (spring constant  $k = 42$  N/m) from Olympus Corporation (Hamburg, Germany) are used.

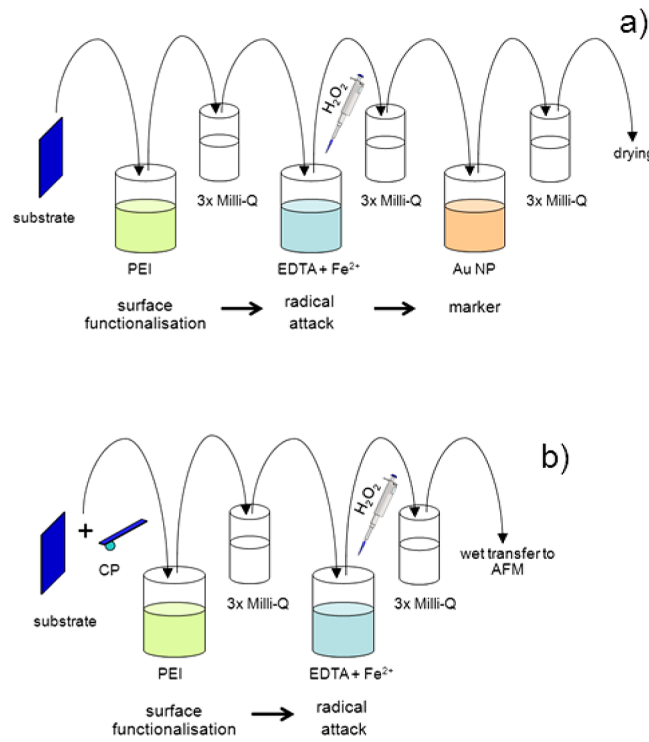
For colloidal probe (CP) force measurements a silica sphere (radius  $R \approx 2.5 \mu\text{m}$ , determined with optical microscopy; purchased from Bangs Laboratories, Fishers, IN) is glued with UV-curable epoxy (NOA68, Norland Adhesives, Cranbury, NJ) onto CSC12 cantilevers (spring constant  $k = 0.005\text{--}0.03$  N/m; MicroMasch, Tallin, Estonia). CP cantilevers are cleaned with argon Plasma Cleaner/Sterilizer PDC-3XG (35 W for 1 min, Harrick Scientific, NY) and are used immediately for force measurements. All force measurements (including the force volume measurements) are performed in an AFM liquid cell containing a sodium chloride solution (NaCl from Merck, Darmstadt, Germany).

**X-ray Photoelectron Spectroscopy (XPS).** XPS is used to investigate the chemical composition of the PEI layers (freshly prepared and after radical attack). The core spectra are recorded with a VG Microtech spectrometer (VG Microtech, W. Sussex, UK) equipped in twin anode X-ray source and a hemispherical photoelectron energy CLAM-2 analyzer. The pressure in the analysis chamber is kept for all measurements at  $10^{-6}$  Pa. The samples under investigation are exposed to a Mg K $\alpha$  X-ray source at 100 W (10 kV, 10 mA) to generate the photoelectron beam. The energy analyzer is located directly above the sample; the angle between the analyzer and the X-ray source is  $54.7^\circ$ .

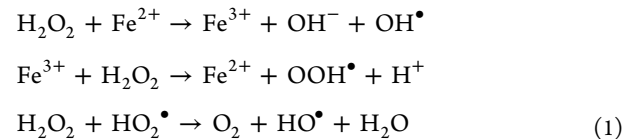
Overview scans (100–1253.6 eV) are recorded in the constant energy mode with a pass energy of 50 eV and resolution of 0.5 eV.<sup>15</sup> Detailed scans have a resolution of 0.05 eV. The peak areas are analyzed with the program package XpsPeak Fit 4.1.

**AFM Imaging, Sample Preparation, Data Analysis.** Microscope slides are cleaned according to the RCA standard and freshly used. The surface functionalization and treatment is shown in Scheme 1a: silica slides are placed into salt free 3 mM PEI solution for 45 min. After washing the slides three times in clean water, they are immersed into a beaker with  $Fe^{2+}$ -EDTA solution. To produce hydroxyl radicals (Fenton's reaction

**Scheme 1.** (a) Sample Preparation for AFM Tapping Mode Imaging in Air and (b) Substrate and CP Preparation for AFM Force Measurements in a Liquid Cell



shown in eq 1), a pipet is used to bring the  $H_2O_2$  solution into the beaker, about 5 mm above the PEI covered slide.



After a reaction time of 5 min, the slide is washed three times in Milli-Q water and immersed into a marker solution containing AuNPs, which are used as markers to investigate PEI layer homogeneity after the radical attack. AuNPs are negatively charged and adsorb onto a positively charged surface. The surface coverage of the AuNPs is systematically varied by using different adsorption times.<sup>16–19</sup> Afterward, the sample is washed again three times in Milli-Q water and dried in a laminar flow box (BDK Luft- und Reinraumtechnik GmbH, Sonnenbühl-Genkingen, Germany). The AuNPs on PEI-functionalized surfaces are imaged with AFM tapping mode in air (ambient conditions). To quantify the AuNP surface coverage  $\Gamma(t)$  at least three different areas of every sample are imaged.

Assuming that each AuNP adsorbs onto the surface, when it arrives there, the surface coverage depends on the AuNP concentration  $c_0$  and the diffusion constant of the AuNP in the solution  $D_{\text{Bulk}}$  as well as the adsorption time  $t$ .<sup>16</sup>

$$\Gamma(t) = 2c_0\sqrt{\frac{D_{\text{Bulk}}t}{\pi}} \quad (2)$$

Here  $c_0 = 1.44 \times 10^{18} \text{ NPs}/\text{m}^3 = 1.44 \text{ NPs}/\mu\text{m}^3$  which corresponds to 2.4 nM for the AuNP solution used.<sup>17</sup> The diffusion constant of a sphere with radius  $r$  in water with the viscosity  $\eta$  is given by the Stokes–Einstein equation

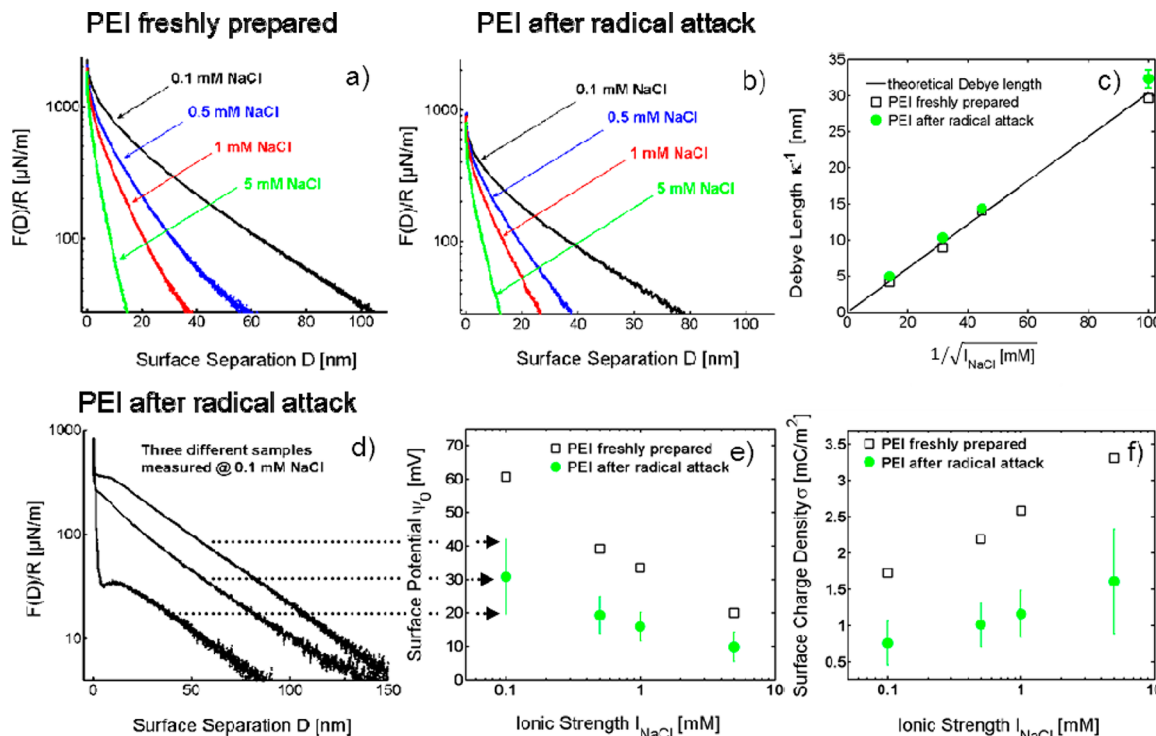


**Figure 1.** (a, b) Force profiles (of freshly prepared PEI adsorption layer and after radical attack) decay exponentially at larger distances ( $d > 3$  nm for 5 mM;  $d > 30$  nm for 0.1 mM); the decay lengths are given in panel c. In both cases, the same decay length (symbols) is observed for a given  $I_{\text{NaCl}}$ , which matches with the expected Debye length (line). Hence, a repulsive electrostatic force dominates the interaction and PEI appears as a flat layer (on length scales  $> 1$  nm). (d) Force curves recorded in 0.1 mM NaCl for three different PEI samples after radical attack decay with the same Debye length ( $\kappa^{-1} \approx 32$  nm) but differ in the magnitude of the electrostatic force. This indicates that the three samples exhibit different surface potentials after radical attack. (e) Surface potentials are obtained by fitting the measured force profiles according to the Debye – Hückel theory. After radical attack, they are reduced by a factor of 0.5. Please note that the green dots result from 10 independently prepared samples (approximately 3000 single force profiles). (f) The surface charge density (calculated using Grahame’s equation and the surface potentials of panel e) also decreased by a factor of 0.5 after radical attack.

$$D_{\text{Bulk}} = \frac{k_B T}{6\pi\eta r} \quad (3)$$

To quantify the AuNP surface coverage, we employ the following approach.<sup>20,21</sup> With a home-written MatLab script (MathWorks, Natick, MA) the AFM images are scanned for local maxima, which are assumed to be the apexes of the NPs. The (thus determined) lateral positions of the apexes are stored and marked by a circle in the images. Using this data, we calculate the NP surface coverage for each AFM image by counting the number of detected AuNPs per unit area.

**AFM Force Measurements, Sample Preparation, Data Analysis.** The sample preparation for force measurements is shown in Scheme 1b. First, the silica microscope slides are RCA cleaned and the CPs are cleaned using argon plasma. Silica slides and CPs are coated with PEI as described in the last section. Also, the reaction with ROS and the subsequent removal of the salt solution by washing in clean water is performed the same way. Both the CPs and the substrate are transferred immediately, without drying, into the AFM liquid cell (wet transfer). In the case of force volume measurements Si wafers serve as substrates, since they exhibit a much lower surface roughness (1.7 Å) than silica slides (4.0 Å).<sup>8</sup>

Force measurements are performed at different NaCl concentrations (0.1–5 mM). For every concentration about 250 single force profiles on at least three different positions on the surface are measured. All in all over 40 000 single force profiles are recorded. The spring constants are determined by

analyzing the thermal noise spectra in air, after recording the force profiles.<sup>22–24</sup>

Single force curves as well as force volume measurements (i.e., spatially resolved force curves = force map) are acquired. From these measurements, the surface potential and surface charge density are determined. Force volume measurements are performed on an  $30 \times 30 \mu\text{m}^2$  area, which is dissected into a grid of  $16 \times 16$  pixel<sup>2</sup> (= lateral resolution of 2 μm/pixel, comparable to the CP radius  $R \approx 2.5 \mu\text{m}$ ).

The force distance profiles are calculated from the displacement of the piezo crystal and the cantilever deflection (using the spring constant). Zero separation is obtained from the onset of the constant compliance region. The interaction force  $F(D)$  (at separation  $D$ ) is measured while approaching the surfaces and normalized by the radius  $R$  of the colloidal probe.

Derjaguin’s approximation shows that the force  $F(D)$  between a spherical particle with the radius  $R$  and a planar surface is proportional to the interaction energy per unit area  $w(D)$  of two planar surfaces<sup>25</sup>

$$F(D) = 2\pi R w(D) \quad (4)$$

The measured interaction force is analyzed assuming two homogeneously charged surfaces in an aqueous solution ( $F_{\text{el}}(D)$ ); that is, van der Waals forces or steric forces are not taken into account.

$$F(D) = F_{\text{el}}(D) = F_0 e^{-\kappa D} \quad (5)$$

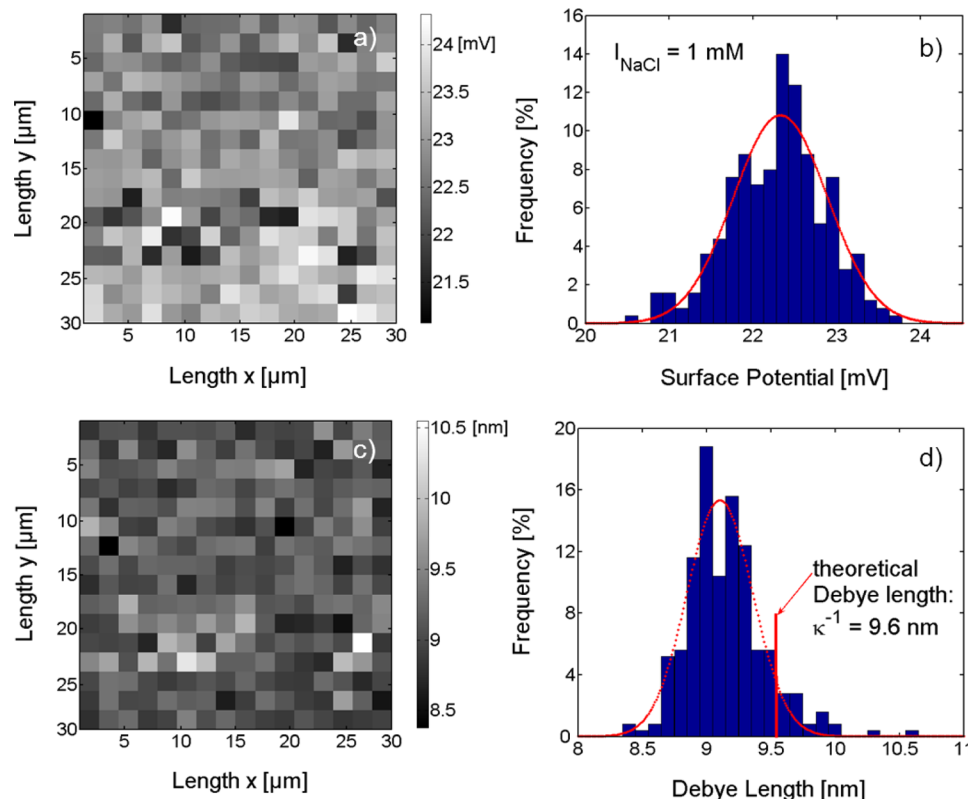


**Figure 2.** Shown are maps ( $30 \times 30 \mu\text{m}^2$ ) and distribution histograms of the surface potential (a and b) and the Debye length (c and d) obtained by AFM force volume measurements on radical attacked PEI layers for  $I_{\text{NaCl}} = 1 \text{ mM}$  (parameters were derived similar to Figure 1, panels c and e). The surface potential shows a Gaussian distribution with an average at 22.3 mV and a standard deviation of 0.56 mV. The Debye length exhibits also a Gaussian distribution (average = 9.2 nm; standard deviation 0.31 nm).

The Debye length  $\kappa^{-1}$  for monovalent salts at 25 °C can be calculated with eq 6.

$$\kappa^{-1} = \frac{0.3 \text{ nm}}{\sqrt{I_{\text{NaCl}}}} \quad (6)$$

The surface potential  $\psi_0$  is derived from a least mean square fit of the measured force (at sufficiently large separation  $D$  as necessary for the Debye–Hückel approximation):<sup>25</sup>

$$\frac{F_{\text{el}}(D)}{2\pi R} = 0.064 \frac{N_A k_B T I_{\text{NaCl}}}{\kappa} \tanh^2 \left( \frac{e\psi_0}{4k_B T} \right) e^{-\kappa D} = \frac{F_0}{2\pi R} e^{-\kappa D} \quad (7)$$

with  $N_A$  being Avogadro's constant. The surface charge density  $\sigma_0$  is calculated from the surface potential using Grahame's equation for solutions containing only monovalent salts:<sup>25</sup>

$$\sigma = \sqrt{8\epsilon\epsilon_0 k_B T} \sinh \left( \frac{e\psi_0}{2k_B T} \right) \sqrt{I_{\text{NaCl}}} \quad (8)$$

## RESULTS

**PEI Surface Forces.** The effect of a hydroxyl radical attack is investigated by recording and analyzing surface force profiles arising between two adsorbed PEI layers before and after radical attack. PEI adsorbs as a flat monolayer (on a length scale  $>1 \text{ nm}$ ) onto a silicon surface.<sup>10</sup> The surface forces are measured in aqueous solution, while the NaCl concentration is varied. The force profiles between freshly prepared PEI layers and PEI layers after radical attack are shown in Figure 1a,b,

respectively. Both measurement series show a strong repulsive interaction which decays exponentially at sufficiently large distances ( $D > 3 \text{ nm}$  for 5 mM NaCl;  $D > 30 \text{ nm}$  for 0.1 mM NaCl) as expected from eq 5. Furthermore, the range of the force profiles (as indicated by their decay length) increase with decreasing salt concentration in solution.

To verify the idea that the surface forces can be described as electrostatic forces, the experimentally determined decay lengths are compared to the theoretically predicted Debye length in dependence of the salt concentration  $I_{\text{NaCl}}$  (cf. Figure 1c, and Figure S1 in the Supporting Information). A good agreement for each salt concentration is found. Furthermore, the measured decay lengths are not affected by a radical attack (i.e., the factor  $e^{-\kappa D}$  in eq 5 is valid before and after the radical attack).

However, it is apparent from a comparison of Figure 1a,b that the radical attack reduces the magnitude of the repulsion (i.e.,  $F_0$  of eq 5 is decreased after radical attack). Figure 1d shows three examples of force curves after radical attack measured for three different PEI samples in 0.1 mM NaCl solution. Although the profiles decay with the same Debye length, they differ strongly in the magnitude of the repulsive electrostatic forces.

Figure 1e shows the surface potentials before and after radical attack in dependence of  $I_{\text{NaCl}}$ , which are determined by fitting eq 7 to the measured force profiles. Both surface potentials, before and after a radical attack, decrease with increasing  $I_{\text{NaCl}}$ . Generally, the surface potentials after radical attack are reduced by a factor of 0.5 in comparison to the surface potential of freshly prepared PEI layers (i.e., the courses

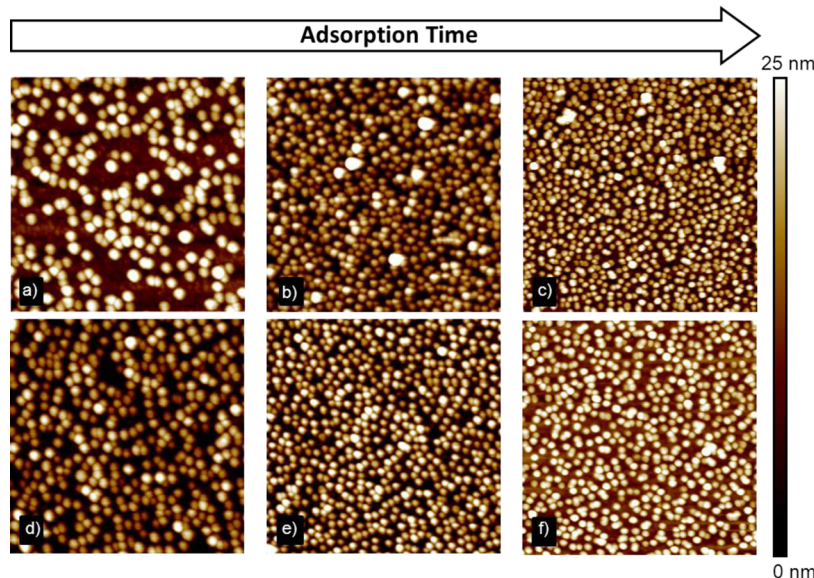


**Figure 3.** AFM tapping mode images ( $1 \times 1 \mu\text{m}^2$ ) of gold nanoparticles (AuNPs; radius = 8 nm) adsorbed onto PEI layers for different adsorption times as indicated. The Au NPs are either adsorbed onto (a–c) freshly prepared PEI or (d–f) PEI after radical attack. The surface coverage  $\Gamma(t)$  for different adsorption times is (a)  $\Gamma(50 \text{ min}) = 247 \text{ NP}/\mu\text{m}^2$ , (b)  $\Gamma(90 \text{ min}) = 501 \text{ NP}/\mu\text{m}^2$ , (c)  $\Gamma(20 \text{ h}) = 769 \text{ NP}/\mu\text{m}^2$ , (d)  $\Gamma(50 \text{ min}) = 328 \text{ NP}/\mu\text{m}^2$ , (e)  $\Gamma(90 \text{ min}) = 532 \text{ NP}/\mu\text{m}^2$ , and (f)  $\Gamma(20 \text{ h}) = 689 \text{ NP}/\mu\text{m}^2$ . All measurements are performed in air. The apparent variation of the AuNP shape is due to AFM tip convolution effects.

of the surface potentials in dependence of  $I_{\text{NaCl}}$  are qualitatively the same, but after radical attack it is shifted downward by a factor of 0.5). The error bars in Figure 1e indicate the scattering of the surface potential observed for several repetitions of the measurements using independently prepared surfaces. The surface potential generally scatters by approximately 30% of its average value.

However, Figure 1f shows that the surface charge density (as calculated by applying eq 8 to the surface potentials) increases with increasing  $I_{\text{NaCl}}$ . Again, the courses are qualitatively the same and a reduction by a factor of 0.5 is observed after radical attack. Similar to the surface potentials, a large scattering of the surface charge density of approximately 30% is found for PEI layers.

With increasing salt concentration the surface potential decreases and the surface charge increases. Therefore, charge regulation occurs. The increase of the salt concentration leads to dissociation of the amines of the PEI.<sup>25</sup> This behavior differs from Si surfaces, which exhibit roughly a constant surface charge, independent of the salt concentration. After exposure to ROS, the surface potential and the surface charge are both reduced. However, their dependence on the salt concentration is similar, indicating that the charge regulation mechanism is unchanged. This suggests that the reaction with ROS may cleave amine groups from the PEI but does not add any dissociating side group.

Please note that control experiments showed none of the discussed effects if the PEI layers were exposed to various solutions with the components necessary for the radical attack, yet without hydrogen peroxide. This means that the PEI layers behaved in these control experiments like the freshly prepared PEI layers.

To determine whether the scattering in surface potential/charge density after radical attack is caused by inhomogeneities within a single surface or by variations of the radical attacks from sample to sample, spatially resolved AFM force volume measurements are performed at 1 mM NaCl. The measure-

ments are analyzed in the same way as force profiles shown in Figure 1a,b. Figure 2a shows a map ( $30 \times 30 \mu\text{m}^2$ ) of surface potentials of a PEI layer after radical attack. Each pixel ( $16 \times 16$  pixels with a pixel size of  $1.875 \times 1.875 \mu\text{m}^2$ ) represents one value of the surface potential, which is obtained from a surface profile measured at the position indicated. Therefore, the map shows the lateral distribution of the surface potential on the sample surface. In a similar way, a map of the Debye length measured at every pixel after radical attack is shown (Figure 2c). As expected, the Debye length is almost constant and shows a Gaussian distribution around 9.2 nm (theoretically expected 9.6 nm) and a standard deviation of 0.31 nm (cf. Figure 2d).

Interestingly, the surface potential exhibits also a Gaussian distribution (Figure 2b) with an average of 22.3 mV and a standard deviation of 0.56 mV (i.e., with a scattering of about 2.5%; in comparison to 30% scattering from sample to sample). The surface potential map (Figure 2a) shows therefore a homogeneous distribution (in the range of 1–2 mV) on  $30 \times 30 \mu\text{m}^2$ . This is very similar to freshly prepared PEI layers (cf. Figure S2 in the Supporting Information), which also exhibit a Gaussian distribution around 32.7 mV with a small standard deviation of 0.7 mV (~ 2.1% of the average value). Therefore, the scattering of surface potential (and also of the surface charge density) results from a variation from sample to sample, indicating that the efficiency of the PEI deposition process and/or of the radical reaction varies strongly between independently prepared surfaces.

**Adsorption of Au Nanoparticles.** In addition to the force volume measurements, adsorption of gold nanoparticles (AuNPs) onto PEI layers was conducted to test the lateral distribution of the surface charge density after radical attack for inhomogeneities on the nm-scales (force volume measurements:  $R = 2.5 \mu\text{m}$ , area size  $30 \times 30 \mu\text{m}^2$ ; AuNP adsorption:  $r = 8 \text{ nm}$ , area size  $1 \times 1 \mu\text{m}^2$ ). Moreover, measurement of force profiles allows us to determine the decrease in surface potential induced by the radical attack, but it does not allow to infer the

actual sign of the surface potential and if the PEI layer is still positively charged after radical attack.

Figure 3 gives six representative AFM images ( $1 \times 1 \mu\text{m}^2$ ) of PEI layers covered with AuNPs. Figure 3a–c shows freshly prepared PEI surfaces, which are covered with AuNPs for three different adsorption times. The surface coverage  $\Gamma(t)$  of AuNPs increases with increasing adsorption time (247 NP/ $\mu\text{m}^2$  after 50 min, 501 NP/ $\mu\text{m}^2$  after 90 min, 769 NP/ $\mu\text{m}^2$  after 20 h). Figure 3d–e shows AuNPs adsorbed onto radical attacked PEI layers (while the same adsorption times were used as in Figure 3a–c). As AuNPs generally adsorb electrostatically onto such surfaces,<sup>14</sup> the PEI layer is still positively charged after radical attack.

In the beginning of the adsorption process ( $t < 50$  min), more AuNP adsorbs onto the PEI layer after radical attack than on the freshly prepared PEI layer (for  $t = 50$  min roughly 32% more; cf. Figure 3a,d). However, after 90 min adsorption time the surface coverage is almost the same for both PEI layers (cf. Figure 3b,e). Figure 3c,f indicates the maximum surface coverage (measured after 20 h adsorption time). Due to the radical attack of the PEI layer, the surface coverage is decreased by about 10%. Summarizing, at short adsorption times ( $t < 90$  min) the AuNP adsorb faster onto radical attacked PEI layers, yet the surface coverage increases more slowly for these layers than for freshly prepared PEI layers. Additionally, the maximum surface coverage is larger for freshly prepared PEI layers. At saturation, the surface coverage is homogeneous down to 1300 nm $^2$ , the average area per AuNP (cf. Figure S3 in the Supporting Information). This corresponds to a length scale down to 40 nm.

The quantitative results of Figure 3 and of approximately 60 additional AFM tapping mode images are summarized in Figure 4, which shows the surface coverage of AuNPs versus the

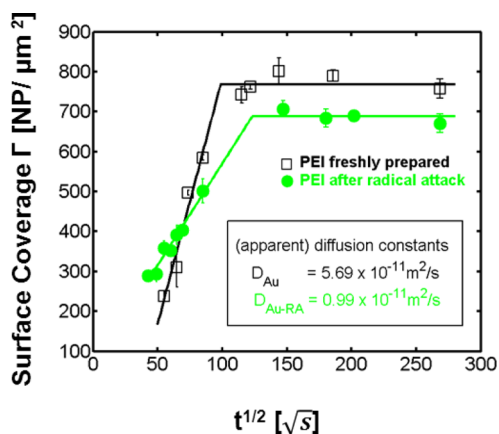


**Figure 4.** Surface coverage of AuNPs versus square root of adsorption time. The AuNPs are adsorbed onto freshly prepared PEI layers (black) or after radical attack (green), respectively; slope and saturation are fitted linearly. The diffusion constants are calculated from the linear slope, according to eq 2.

square root of adsorption time. The black symbols and lines represent measurements done using freshly prepared PEI, while the green symbols and lines correspond to PEI layers after radical attack. The lines (slope and saturation) are obtained by fitting a linear function to the data points. From the slope, an apparent diffusion constant,  $D_{\text{Bulk}}$ , is determined using eq 2.

Schmitt et al.<sup>17</sup> used the concept of diffusion limited adsorption<sup>16</sup> to describe the adsorption of AuNPs onto

oppositely charged surfaces. They showed (using AuNPs of the same size and chemistry as we do) that the coverage of AuNPs adsorbed from  $c_0 = 1.44 \times 10^{18}$  AuNPs/m $^3$  onto positively charged surfaces increases (independent of the surface chemistry) with the square root of the adsorption time until it reaches saturation after 2.8 h. Our work agrees with the results of Schmitt et al. in case of freshly prepared PEI layers. However, Figure 4 shows that the slope decreases if the PEI layers were subject to a radical attack. The apparent diffusion constants for AuNPs adsorption before and after radical attack differ by a factor of 5.8. Furthermore, after radical attack the saturation of AuNP surface coverage occurs at a later adsorption time (4.3 h versus 2.8 h for freshly prepared PEI layers), and the related maximum surface coverage is decreased by roughly 10% with respect to freshly prepared PEI layers.

**X-ray Photoelectron Spectroscopy (XPS).** With the XPS measurements, we investigate if the radical attack changes the chemical composition of the PEI layer (e.g., adsorption of additional ions onto the layer). The different components of Mohr's salt may adsorb onto oppositely charged surfaces. We consider especially Fe<sup>2+</sup> and SO<sub>4</sub><sup>2-</sup>. Figure 5a shows XPS spectra for binding energies ranging from 149.5 to 178 eV for a freshly prepared PEI layer, a PEI layer after radical attack, and a reference sample. All spectra show a Si 2s peak, which is due to the identical Si wafers that served as substrates for the layers. However, the freshly prepared PEI layer and PEI layer after radical attack show only a small S 2p peak. In both cases, the rate of sulfur is round 5%. This means that the radical attack has no influence on the sulfur rate, and no additional adsorption of SO<sub>4</sub><sup>2-</sup> occurs.

Figure 5b depicts XPS spectra for binding energies ranging from 700 to 737 eV. The reference spectrum shows the Fe 2p<sub>3/2</sub> and the Fe 2p<sub>1/2</sub> peak. Neither the freshly prepared PEI layer nor the PEI layer after radical attack show these iron peaks. Hence, the radical attack does not foster the adsorption of iron ions.

Summarizing, the XPS measurements indicate that the chemical composition of the PEI layer is not altered by the radical attack. Further details can be found in Tables 1 and 2 in the Supporting Information.

## DISCUSSION

In this work the effect of a reaction of ROS with a positively charged PEI monolayer is investigated. AFM colloidal probe force measurements on PEI layers are used to determine surface properties (surface potential and surface charge density) before and after radical attack. Only the part of the force curves at large distances is considered, between 3 and 120 nm (cf. Figure S1 in the Supporting Information). Interestingly, the decay length is not affected by the radical attack and generally agrees with the theoretically expected Debye length (cf. Equation 6). These findings confirm the view that the electrostatic repulsion dominates the surface forces at large surface separations.<sup>10</sup> We find no evidence for other forces like steric forces. It follows that the PEI surface is still a flat monolayer after radical attack (on length scale  $>1$  nm). Moreover single chains or brush building events after radical attack can be excluded.<sup>8</sup>

Furthermore, XPS measurements find no evidence for additional ion adsorption onto the PEI layer in consequence of the radical attack (Tables 1 and 2 in the Supporting Information). This indicates that the decreased surface potential/charge density after radical attack is caused by a

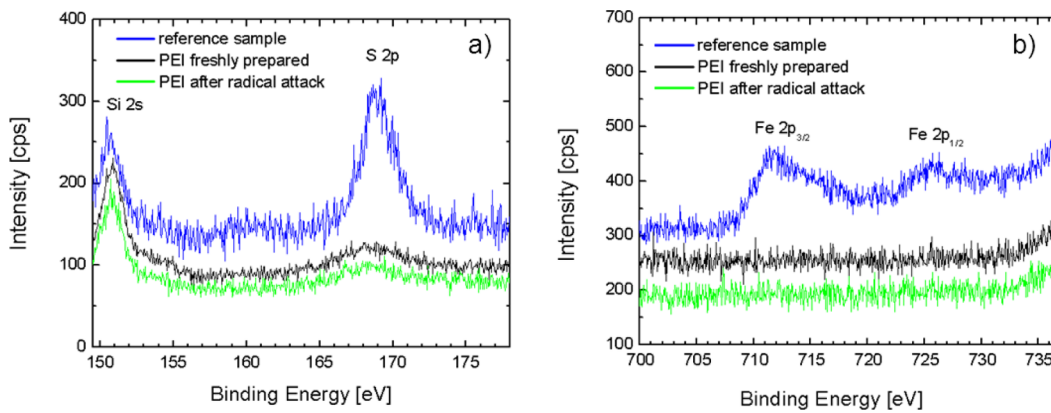


**Figure 5.** XPS spectra of freshly prepared PEI layers (black), radical attacked PEI layers (green), and a reference probe (blue), which contains sulfur and iron. All samples were prepared on silicon. A small vertical shift was introduced between the different spectra to simplify the visual inspection. Panel a gives spectra ranging from 149.5 to 178 eV including the Si 2s (@ 151 eV) and the S 2p peaks (@ 169 eV). In both cases (PEI freshly prepared and after radical attack) the intensity at 169 eV is almost equal. Panel b gives spectra ranging from 700 to 737 eV including two iron peaks. No evidence is found for the presence of iron on freshly prepared or radical attacked PEI layers.

reduction of the effective charge carriers. Since there is no evidence of additional ions, we conclude that the chemical composition of the surface is not affected by radical attack.

Based on the constant Debye length and consequently the constant range of electrostatic force, we observe that the magnitude of the electrostatic repulsion reduces after radical attack. Quantitatively, the radical attack reduces the surface potential and the surface charge density by a factor of 0.5. This suggests that also the effective number of charge carriers is reduced down to 50% by the radical attack.

Furthermore, the surface potential and surface charge density scatter about 30% from sample to sample, suggesting an inhomogeneous distribution of these properties on the PEI layers. AFM force volume measurements show that the hydroxyl radical attack is homogeneous (concerning surfaces potential and surface charge density) within one single sample on length scales up to 30  $\mu\text{m}$ . Additionally, as we also find a homogeneous distribution of gold nanoparticles (AuNPs) on the PEI layers, we concluded that the surface potential/charge density after radical attack is also homogeneous down to a length scale of the AuNP radius ( $r = 8 \text{ nm}$ ). As a consequence we suggest that the hydroxyl radical attack itself proceeds homogeneously within the described dimension. Moreover, the adsorption of negatively charged AuNPs onto oppositely charged PEI layers shows that the PEI surface is still positively charged after a radical attack.

However, there is an apparent contradiction: After the reaction of the PEI layer with the ROS, the apparent diffusion constant of the AuNP in the solution is reduced by a factor of 5. A changed bulk diffusion constant of AuNPs is not likely. Therefore, the assumptions, which lead to eq 2, need a rethink. One of the assumptions is sticking probability of one, which means that each nanoparticle, which touches the surface, immediately sticks to the surface. After the radical attack the surface charge is reduced (due to reduction of positively charged groups and/or addition of negatively charged groups). Hence, the sticking probability is reduced as the AuNPs do not always find suitable binding sites, which decreases the AuNP adsorption rate and apparently decreases the diffusion constant. Note that a reduced sticking probability is only possible, if the surface is laterally inhomogeneous on the scale of a few nm.

Actually, there is a second apparent contradiction: The amount of positively charged binding sites is reduced to 50%

after radical attack (Figure 1c), whereas the saturation limit of AuNP adsorption after radical attack surprisingly reduces by only 10% (AuNP saturation limit freshly prepared:  $769 / \mu\text{m}^2$ , 15.5% of total area; after radical attack:  $689 / \mu\text{m}^2$ , 13.9% of total area). With the help of an extended three-body RSA (random sequential adsorption) model this contradictory adsorption tendency of AuNPs can be explained.<sup>11,12</sup>

In RSA models, it is assumed that a particle adsorbs irreversibly onto a surface. A second particle cannot adsorb (due to steric hindrance) in the direct vicinity of the original particle. The classical two-body RSA model considers only the Coulomb potential arising between two charged particles; the substrate is not taken into account. The extended three-body RSA model goes one step further as it uses a three body Coulomb potential concerning the two charged particles (AuNPs) and the charged substrate (PEI surface):<sup>12</sup>

$$u(a) = \frac{Z^2 e^2}{4\pi\epsilon_w\epsilon_0} \left[ \frac{\exp(\kappa_{\text{eff}}r)}{1 + \kappa r} \right]^2 \frac{\exp(-\kappa_{\text{eff}}a)}{a} \quad (9)$$

Here  $e$  is the elementary charge,  $\epsilon_w\epsilon_0$  is the dielectric permittivity of water,  $r$  is the radius of an AuNP,  $\kappa^{-1}$  is the Debye length of the AuNP solution and  $a$  is the center-to-center separation of two AuNPs.  $Z = (r/L_B)(4\kappa r + 6)$  is the effective AuNP charge (in units of elementary charge; in case of AuNPs  $Z = 156$ , cf. Figure 6),<sup>12</sup> and  $L_B$  is the Bjerrum length,  $L_B = e^2/4\pi\epsilon_0\epsilon_w k_B T \approx 0.72 \text{ nm}$ .

The effective Debye length  $\kappa_{\text{eff}}^{-1}$  of the AuNP solution close to the substrate is defined as<sup>12</sup>

$$\kappa_{\text{eff}} = \kappa \cosh \left( \frac{e\psi_0(I_{\text{NaCl}})}{k_B T} \right) \quad (10)$$

The effective Debye length leads to an effective radius  $r_{\text{eff}}$  of the AuNPs:<sup>12</sup>

$$r_{\text{eff}} = \frac{1}{2\kappa_{\text{eff}}} \ln(A/\ln A) \quad (11)$$

Here  $A$  is a constant,  $A = \lambda Z^2 \kappa L_B \exp(2\kappa_{\text{eff}}r)/(1 + \kappa r)^2$ , and  $\lambda$  is set to 2.8 (numerical calculations).

For the calculation of  $\kappa_{\text{eff}}$  the surface potentials (cf. Table 2, Supporting Information)  $\psi_{0,\text{PEI}}(5 \text{ mM}) = 20.04 \text{ mV}$  (PEI freshly prepared),  $\psi_{0,\text{PEI-RA}}(5 \text{ mM}) = 9.89 \text{ mV}$  (PEI after

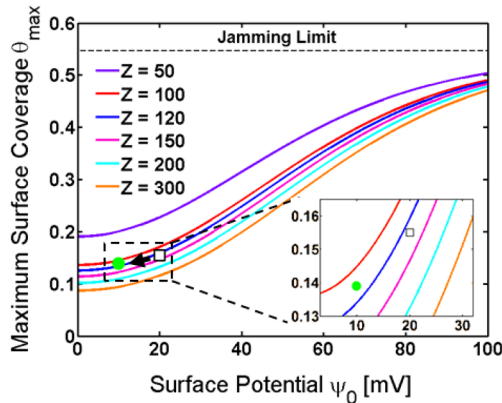


**Figure 6.** Maximum surface coverage  $\Theta_{\max}$  of AuNPs on PEI functionalized surfaces versus PEI surface potential  $\psi_0$ . Colored lines indicate theoretically expected  $\Theta_{\max}$  according to a three body RSA model (cf. eq 9) in dependence of  $\psi_0$  and  $Z$  (the effective AuNP charge in units of elementary charge). The Debye length of the AuNP solution is  $\kappa^{-1} = 3.98$  nm, which corresponds to an ionic strength of  $I_{\text{Au}} = 5.8$  mM (assuming that the AuNP solution is an aqueous 1:1 electrolyte).  $\Theta_{\max}$  increases with increasing  $\psi_0$  and decreasing  $Z$ . The dots are experimental data for (black) freshly prepared and (green) radical attacked PEI layers. The dashed line shows the jamming limit (threshold for particle coverage). All theoretical curves suggest for  $\psi_0 < 20$  mV that a decrease of  $\psi_0$  by 50% causes only a 10–15% reduction of  $\Theta_{\max}$ , which agrees with the experimental data.

radical attack), and the Debye length of the AuNP solution  $\kappa^{-1} = 3.98$  nm are used.<sup>14</sup>

For freshly prepared PEI layers, we obtain an effective Debye length of  $\kappa_{\text{eff,PEI}}^{-1} = 3.01$  nm, and after radical attack of  $\kappa_{\text{eff,PEI-RA}}^{-1} = 3.70$  nm. The corresponding effective radii are  $r_{\text{eff,Au}} = 15.5$  nm (freshly prepared) and  $r_{\text{eff,Au-RA}} = 17.0$  nm (after radical attack).

If one knows the effective particle radius  $r_{\text{eff}}$  the maximum coverage (saturation)  $\Theta_{\max}$  can be calculated by<sup>12</sup>

$$\Theta_{\max} = \Theta_{\text{jam}} \left( \frac{r}{r_{\text{eff}}} \right)^2 \quad (12)$$

The jamming limit  $\Theta_{\text{jam}}$  is the upper limit for the particle coverage and reaches  $\Theta_{\text{jam}} = 0.547$  in the case of spherical particles adsorbed onto hard surfaces. The theoretical maximum coverages for  $I_{\text{NaCl}} = 5$  mM are  $\Theta_{\max} = 14.7\%$  (freshly prepared PEI surfaces) and  $\Theta_{\max} = 12.2\%$  (after radical attack), which agree well with the experimentally determined values of 15.5% (freshly prepared PEI surfaces) and 13.9% (after radical attack).

Figure 6 shows the theoretical saturation limits  $\Theta_{\max}$  of AuNP as function of the surface potential  $\psi_0$  of PEI surfaces and the effective AuNP charge  $Z$  according the extended three-body RSA model (colored lines). The theoretical curves show for all values of  $Z$  the same nonlinear trend. For small  $\psi_0$  ( $< 20$  mV) a 50% reduction of the surface potential  $\psi_0$  causes only a 10–15% reduction of the maximum surface coverage  $\Theta_{\max}$ . The experimental data (solid dots) show the same trend. Therefore we conclude that the nonlinear relationship between surface charge and  $\Theta_{\max}$  of AuNPs can be well described by the extended model.

One might argue that neither the AuNP size ( $r = 8$  nm) nor the salt concentration of the AuNP (5 mM, Debye length 4 nm) are of biological relevance. Therefore, a change of the surface charge of a cell membrane does not necessarily affect the

saturation coverage of adsorbed proteins. Of course, proteins are smaller ( $r = 1–3$  nm) than our AuNPs and biological solutions contain more salt (0.15 M, Debye length 0.7 nm). However, close consideration of the extended three-body RSA model shows that the important parameter is  $r/a$ , and this parameter is approximately 2 in our experiments. One can easily imagine biological scenarios for which  $r/a$  equals 2 and a reaction with ROS of a cell membrane therefore affects the coverage of nonspecifically adsorbed proteins.

## CONCLUSION

Positively charged, branched polyethylenimine (PEI) is adsorbed flatly onto silicon wafers and attacked by free hydroxyl radicals. After the attack, the PEI layers maintain their flat conformation, suggesting that the PEI still has positively charged groups and physisorbs by electrostatic bonds to the substrate. Nevertheless, after radical attack the surface charge density is reduced by a factor of about 0.5, suggesting changes of the chemical composition of the PEI layer. Either positive side groups are cut off or negative side groups are added. The latter is ruled out by XPS measurements, which shows that ions of the reaction solution (Fe and S) do not adsorb onto the substrate.

Investigating different samples, we observed a 30% scattering of the surface charge. Therefore, the lateral homogeneity was investigated on different length scales. Force volume measurements show a laterally homogeneous surface charge in the range between 1.8 and 30  $\mu\text{m}$ . Furthermore, the surface coverage of adsorbed gold nanoparticles indicates that the charge distribution remains homogeneous down to length scales of 40 nm. Therefore, we conclude that the large scattering is caused by samples to sample variations, indicating that the efficiency of the ROS attack and/or the PEI layer deposition varies strongly between independently prepared surfaces. Concerning small length scales, the AuNP adsorption kinetics is slowed down suggesting that after radical attack the PEI layer may be inhomogeneous on length scales below 40 nm.

## ASSOCIATED CONTENT

### Supporting Information

Figure S1 shows two exemplary force profiles of different quality measured with AFM colloidal probe technique. Figure S2 gives Gaussian distributions of surface potentials and Debye lengths of a pristine silica surface and of a freshly prepared PEI layer. Figure S3 addresses the question of the lateral homogeneity of the adsorbed gold nanoparticles, both on freshly prepared PEI layers and after a radical attack. Figure S4 gives XPS overview spectra of a PEI layer, again as prepared and after exposure to radicals. The deduced chemical composition of the respective PEI layers is given in Table 1. This material is available free of charge via the Internet at <http://pubs.acs.org>.

## AUTHOR INFORMATION

### Corresponding Author

\*E-mail: helm@uni-greifswald.de.

### Notes

The authors declare no competing financial interest.

## ACKNOWLEDGMENTS

Financial support of the Graduate School “Studies of the interaction of free oxygen radicals with molecules at electrodes and applications to biochemical and medical systems” of the Alfried Krupp Wissenschafts Kolleg Greifswald and of the BMBF (ZIK-HIKE, BMBF FKZ 03Z2CN11) is appreciated.

## REFERENCES

- (1) Jacob, C.; Winyard, P. G. *Redox signalling and regulation in biology and medicine*; Wiley-VCH: Weinheim, Germany, 2009.
- (2) Halliwell, B.; Gutteridge, J. M. C. *Free radicals in biology and medicine*; Oxford University Press: New York, 1999.
- (3) Ishimura, Y.; Nozaki, M.; Yamamoto, S.; Shimizu, T.; Narumiya, S.; Mitani, F. *Oxygen and Life: Oxygenases, Oxydases and Lipid Mediators. Excerpta Medica. International Congress Series 1233*; Elsevier: Amsterdam, 2002.
- (4) Nowicka, A. M.; Hasse, U.; Sievers, G.; Donten, M.; Stojek, Z.; Fletcher, S.; Scholz, F. Selective Knockout of Gold Active Sites. *Angew. Chem.-Int. Ed.* **2010**, *49*, 3006–3009.
- (5) Gröning, A.; Ahrens, H.; Ortmann, T.; Lawrenz, F.; Brezesinski, G.; Scholz, F.; Helm, C. A. Molecular mechanisms of phosphatidylcholine monolayer solidification due to hydroxyl radicals. *Soft Matter* **2011**, *7*, 6467–6476.
- (6) Berndt, P.; Kurihara, K.; Kunitake, T. Adsorption of Poly(styrenesulfonate) onto an Ammonium Monolayer on Mica: A Surface Forces Study. *Langmuir* **1992**, *8*, 2486–2490.
- (7) Lowack, K.; Helm, C. A. Molecular mechanisms controlling the self-assembly process of polyelectrolyte multilayers. *Macromolecules* **1998**, *31*, 823–833.
- (8) Block, S.; Helm, C. A. The conformation of PSS layers physisorbed from high salt solution studied by force measurements on two different length scales. *J. Phys. Chem. B* **2008**, *112*, 9318–9327.
- (9) Block, S.; Helm, C. A. Equilibrium and nonequilibrium factors determining the morphology in physisorbed PSS layers. *J. Phys. Chem. B* **2011**, *115*, 7301–7313.
- (10) Pericet-Camara, R.; Papastavrou, G.; Behrens, S. H.; Helm, C. A.; Borkovec, M. Interaction forces and molecular adhesion between pre-adsorbed poly(ethylene imine) layers. *J. Colloid Interface Sci.* **2006**, *296*, 496–506.
- (11) Adamczyk, Z.; Warszynski, P. Role of electrostatic interactions in particle adsorption. *Adv. Colloid Interface Sci.* **1996**, *63*, 41–149.
- (12) Cahill, B. P.; Papastavrou, G.; Koper, G. J. M.; Borkovec, M. Adsorption of poly(amido amine) (PAMAM) dendrimers on silica: Importance of electrostatic three-body attraction. *Langmuir* **2008**, *24*, 465–473.
- (13) Turkevich, J.; Stevenson, P. C.; Hillier, J. A Study of the Nucleation and Growth Processes in the Synthesis of Colloidal Gold. *Faraday Soc. Discuss.* **1951**, *11*, 55–75.
- (14) Eck, D. *Optische Methoden zur Charakterisierung von Nano-Kolloiden und Polymeren*; Ph.D. Thesis, Universität des Saarlandes: Saarbrücken, Germany, 2000.
- (15) Stranak, V.; Wulff, H.; Bogdanowicz, R.; Drache, S.; Hubicka, Z.; Cada, M.; Tichy, M.; Hippler, R. Growth and properties of Ti-Cu films with respect to plasma parameters in dual-magnetron sputtering discharges. *Eur. Phys. J. D* **2011**, *64*, 427–435.
- (16) Andrade, J. D. *Surface and Interfacial Aspects of Biomedical Polymers*; Plenum Press: New York, 1985; Vol. 1: Surface Chemistry and Physics.
- (17) Schmitt, J.; Mächtle, P.; Eck, D.; Möhwald, H.; Helm, C. A. Preparation and Optical Properties of Colloidal Gold Monolayers. *Langmuir* **1999**, *15*, 3256–3266.
- (18) Adamczyk, Z.; Michna, A.; Szaraniec, M.; Bratek, A.; Barbasz, J. Characterization of poly(ethylene imine) layers on mica by the streaming potential and particle deposition methods. *J. Colloid Interface Sci.* **2007**, *313*, 86–96.
- (19) Adamczyk, Z.; Jaszczolt, K.; Michna, A.; Siwek, B.; Szyk-Warszynska, L.; Zembala, M. Irreversible adsorption of particles on heterogeneous surfaces. *Adv. Colloid Interface Sci.* **2005**, *118*, 25–42.
- (20) Stranak, V.; Block, S.; Drache, S.; Hubicka, Z.; Helm, C. A.; Jastrabik, L.; Tichy, M.; Hippler, R. Size-controlled formation of Cu nanoclusters in pulsed magnetron sputtering system. *Surf. Coat. Technol.* **2011**, *205*, 2755–2762.
- (21) Cornelsen, M.; Helm, C. A.; Block, S. Destabilization of Polyelectrolyte Multilayers Formed at Different Temperatures and Ion Concentrations. *Macromolecules* **2010**, *43*, 4300–4309.
- (22) Butt, H. J.; Jaschke, M. Calculation of thermal noise in atomic force microscopy. *Nanotechnology* **1995**, *6*, 1–7.
- (23) Hutter, J. L.; Bechhoefer, J. Calibration of Atomic-Force Microscope Tips. *Rev. Sci. Instrum.* **1993**, *64*, 1868–1873.
- (24) Cleveland, J. P.; Manne, S.; Bocek, D.; Hansma, P. K. A Nondestructive Method for Determining the Spring Constant of Cantilevers for Scanning Force Microscopy. *Rev. Sci. Instrum.* **1993**, *64*, 403–405.
- (25) Israelachvili, J. N. *Intermolecular and Surface Forces*, 2nd ed.; Academic Press: London, 1991.